Rapid communication

Mössbauer spectroscopy analysis of ^{57}Fe-doped $YBaCo_4O_{7+\delta}$: Effects of oxygen intercalation

E.V. Tsipis [a,b], J.C. Waerenborgh [a], M. Avdeev [c], V.V. Kharton [b,*]

[a] Chemistry Department, Instituto Tecnológico e Nuclear, CFMC-UL, EN 10, 2686-953 Sacavém, Portugal
[b] Department of Ceramics and Glass Engineering, CICECO, University of Aveiro, 3810-193 Aveiro, Portugal
[c] Bragg Institute, Australian Nuclear Science and Technology Organization, PMB 1, Menai, NSW 2234, Australia

ABSTRACT

Mössbauer spectroscopy of layered $YBaCo_{3.96}Fe_{0.04}O_{7+\delta}$ ($\delta = 0.02$ and 0.80), where 1% cobalt is substituted with ^{57}Fe isotope, revealed no evidence of charge ordering at 4–293 K. The predominant state of iron cations was found trivalent, irrespective of their coordination and oxygen stoichiometry variations determined by thermogravimetric analysis. The extremely slow kinetics of isothermal oxidation at 598 K in air, and the changes of Fe^{3+} fractions in the alternating triangular and Kagomé layers in oxidized $YBaCo_{3.96}Fe_{0.04}O_{7.80}$, may suggest that oxygen intercalation is accompanied with a substantial structural reconstruction stagnated due to sluggish cation diffusion. Decreasing temperature below 75–80 K leads to gradual freezing of the iron magnetic moments in inverse correlation with the content of extra oxygen. The formation of metal–oxygen octahedra and resultant structural distortions extend the temperature range where the paramagnetic and frozen states co-exist, down to 45–50 K.

© 2008 Elsevier Inc. All rights reserved.

1. Introduction

Oxide materials derived from recently discovered $RBaCo_4O_7$ (R=Ho, Y) phases [1,2] attract growing interest due to their unusual oxygen-sorption and transport properties, complex structural relationships and frustrated magnetism [2–13]. The crystal structure of these compounds is built of closely packed alternating triangular and Kagomé layers of corner-sharing $Co1O_4$ and $Co2O_4$ tetrahedra, respectively (Fig. 1a), with R and Ba occupying octahedral and anti-cubooctahedral sites. However, reports on finer details of this crystal structure, its temperature evolution and magnetic behavior are quite contradictory. Originally, the structure of $RBaCo_4O_7$ (R=Ho, Y) at room temperature was described by the $P6_3mc$ space group on the basis of X-ray single crystal diffraction and neutron powder diffraction on ground single crystals [1,2]. Later, however, Y [7,9] and Yb [8] analogues were reported to have $P31c$ space group at room temperature with a first-order phase transition to $Pbn2_1$ orthorhombic form occurring at 313 and 175 K, respectively. The Co^{3+} and Co^{2+} cations were suggested to be statistically distributed between the $Co1$ and $Co2$ sites having the concentration ratio of 1:3 [7,8] and to have a preference of Co^{3+} for the $Co1$ sites [1,2]. Analogously, diffuse magnetic scattering in $YBaCo_4O_7$ was

detected in a wide temperature range with long-range three-dimensional antiferromagnetic ordering below 110 K [7]; on the contrary, other authors observed only a short-range order of cobalt magnetic moments at 10 K [10] and a spin–glass state below 65 K [2].

In addition to the uncertainties resulting from the comparison of single crystal's and powder's behavior, the controversies on structural transition(s) and magnetic ordering processes in $YBaCo_4O_7$ seem associated, at least to a significant extent, with oxygen stoichiometry-related factors [3,7]. In particular, annealing of $YBaCo_4O_{7+\delta}$ at 523–623 K in air or flowing O_2 rises the oxygen excess up to $\delta = 1.25$; further heating above approximately 673 K leads to desorption of the extra oxygen [4,6,14]. When hyper-stoichiometric oxygen is intercalated in the lattice of $RBaCo_4O_{7+\delta}$ (R = Y, Yb), increasing average oxidation state and coordination of cobalt cations was reported to suppress the structural transition and magnetic ordering [3,5,7,8]. The high-resolution neutron diffraction and synchrotron X-ray powder diffraction analyses [3] showed that in $YBaCo_4O_8$, the extra oxygen anions order in a doubled unit cell superstructure (S.G. $Pbc2_1$) with a substantial displacement of several oxygen sites to allow increasing coordination number of some Co atoms up to 6 (Fig. 1b). This super-structure involves six tetrahedral and two octahedral Co sites; the tetrahedra remain corner-sharing, while the octahedra share their edges. In the case of $YBaCo_4O_{8.2}$ investigated by X-ray diffraction (XRD) and X-ray absorption near-edge structure (XANES) techniques, a $Pnna$ symmetry was reported [11]. Recently, the
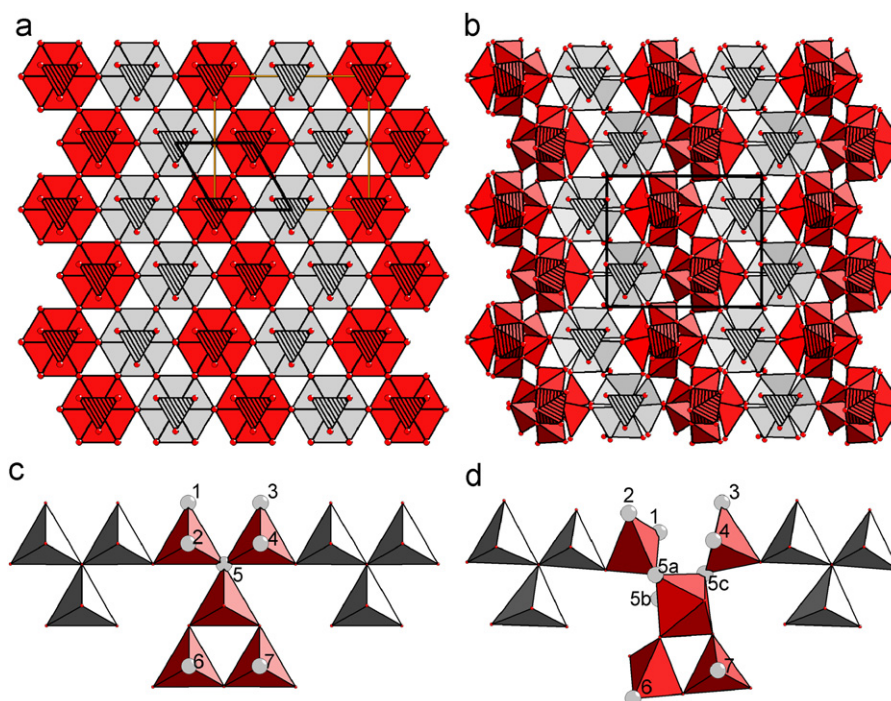
Fig. 1. Top view of $YBaCo_4O_7$ (a) and $YBaCo_4O_8$ (b) crystal structures on the basis of X-ray and neutron diffraction data [2,3]. Y and Ba atoms are omitted for clarity. The fragments having oxidation-unaffected topology, undergoing only a slight polyhedra tilt, are emphasized by gray color. The two-dimensional blocks where the tetrahedra are transformed into octahedra, are shown red. Thick solid lines indicate the hexagonal (a) and orthorhombic (b) unit cells. Hatched and plain faces show the coordination polyhedra of $Co1$ and $Co2$ in $YBaCo_4O_7$ (a), and $Co1(1-2)$ and $Co2(1-6)$ in $YBaCo_4O_8$ (b), respectively. (c) and (d) illustrate the mechanism of extra oxygen insertion into the Kagomé layer of $YBaCo_4O_{7+\delta}$ structure. The oxygen position (5) indicated by light gray color splits into three sites that transform the tetrahedron vertex into the octahedron face, displacing the adjacent oxygen atoms from their ideal positions.

composition with cobalt fully oxidized to the 3+ oxidation state, $YBaCo_4O_{8.5}$, was prepared but its crystal structure was apparently not solved [15].

Irrespective of the existence of $YBaCo_4O_{8.5}$ phase below 673 K [3,4,8], the oxygen uptake at 1000–1200 K causes complete decomposition of $YBaCo_4O_{7+\delta}$ into a mixture of perovskite-like phases and Co_3O_4; the decomposition is accompanied by a conductivity jump and dramatic volume contraction [4,12,13]. At atmospheric oxygen pressure, therefore, the $YBaCo_4O_7$-based compounds appear thermodynamically stable only above approximately 1123–1173 K and metastable at lower temperatures.

Another important feature of $YBaCo_4O_{7+\delta}$ relates to the high solubility of iron in the cobalt sublattice [12], which makes it possible to introduce a probe of ^{57}Fe isotope and to study local structural features and magnetic interactions by the ^{57}Fe Mössbauer spectroscopy (MS). The present work was focused on the analysis of the Mössbauer transmission spectra of essentially oxygen-stoichiometric and oxidized $YBaCo_4O_{7+\delta}$ doped with 1% ^{57}Fe, in combination with thermogravimetry.

2. Experimental

The powders of $YBaCo_{3.96}Fe_{0.04}O_{7+\delta}$ with $\delta = 0.02$ and 0.80 were prepared via glycine–nitrate process (GNP) [16], followed by annealing in air at 1273–1473 K with several intermediate grinding steps. In the course of GNP, the stoichiometric amount of metallic iron enriched with ^{57}Fe isotope (chemical purity 99.96%, ^{57}Fe content 95.73%, Chemgas, France) was dissolved in diluted nitric acid and then added in an aqueous glycine–nitrate solution containing the metal cations in calculated proportions. After synthesis, the samples were finally annealed at 1323 or 598 K and quenched; the thermal treatment conditions and the

resultant oxygen content determined by thermogravimetric analysis (TGA) are given in Table 1.

TGA was carried out using a Setaram SetSys 16/18 instrument (weight resolution of 0.4 μg; noise level of 1.6 μg; sample weight of ∼500 mg). The measurement procedure (Fig. 2) included fast heating in flowing dry air up to 598 or 1323 K, dwells during 3–100 h for equilibration at atmospheric oxygen pressure, flushing the apparatus with argon at 1323 K, and final reduction in flowing 10% H_2–90% N_2 mixture at 1323–1423 K. Room temperature XRD patterns were recorded using a Rigaku D/Max-B diffractometer (Cu$K\alpha$ radiation, $2\theta = 10$–$100°$, step 0.015–0.020°, 3–8 s/step). The XRD analysis of $YBaCo_{3.96}Fe_{0.04}O_{7.02}$ obtained by quenching after annealing at 1323 K, revealed no essential structural changes with respect to Fe-free stoichiometric $YBaCo_4O_7$ [1–5]. On the contrary, the superstructure reflections characteristic of $YBaCo_4O_8$ [3] are clearly present in the XRD pattern of $YBaCo_{3.96}Fe_{0.04}O_{7.80}$ oxidized at 598 K (inset of Fig. 2).

The Mössbauer spectra were collected at 4–293 K using a standard constant-acceleration spectrometer equipped with a ^{57}Co (Rh) source. A JANIS SVT-400 cryostat was used for measurements at 40–80 K and at 4 K with the sample in He exchange gas flow or immersed in liquid He, respectively. The spectra, all referenced to α-Fe at room temperature, were fitted to Lorentzian lines [17] or to static distributions of hyperfine field (B_{hf}) in order to simulate the magnetic relaxation signal [18].

3. Results and discussion

Fig. 3 presents the Mössbauer spectra of $YBaCo_{3.96}Fe_{0.04}O_{7.02}$ and $YBaCo_{3.96}Fe_{0.04}O_{7.80}$, recorded in the temperature range from 293 to 4 K. Both materials are in a paramagnetic state at room temperature, whereas at 4 K, magnetically split patterns are observed. Consequently, the spectra of $YBaCo_{3.96}Fe_{0.04}O_{7.02}$

Table 1
Parameters[a] estimated from the Mössbauer spectra of $YBaCo_{3.96}$ $^{57}Fe_{0.04}O_{7+\delta}$.

Composition	Thermal treatment	Measurement temperature (K)	Iron coordination	IS (mm/s)	QS, ε (mm/s)	B_{hf} (T)	I (%)
$YBaCo_{3.96}Fe_{0.04}O_{7.02}$	$T = 1323$ K, $p(O_2) = 0.21$ atm, 5 h	293	4	0.18	0.54	–	39
			4	0.19	0.37	–	61
		73	4	0.30	0.49	–	40
			4	0.30	−0.06	23.3	60
		4	4	0.30	−0.10	44.3	39
			4	0.30	0.00	41.3	61
$YBaCo_{3.96}Fe_{0.04}O_{7.80}$	$T = 598$ K, $p(O_2) = 0.21$ atm, 18 h	293	6	0.24	0.96	–	28
			4	0.21	0.60	–	31
			4	0.20	0.31	–	41
		60	6	0.36	0.91	–	24
			4	0.30	−0.13	19.5	76
		4	6	0.34	−0.06	44.2	26
			4	0.30	−0.01	42.3	33
			4	0.31	−0.10	40.0	41

[a] IS, B_{hf}, QS, ε and I are the isomer shift, magnetic hyperfine field, quadrupole splitting in a quadrupole doublet, quadrupole shift in a magnetic sextet or distribution, and relative area, respectively.
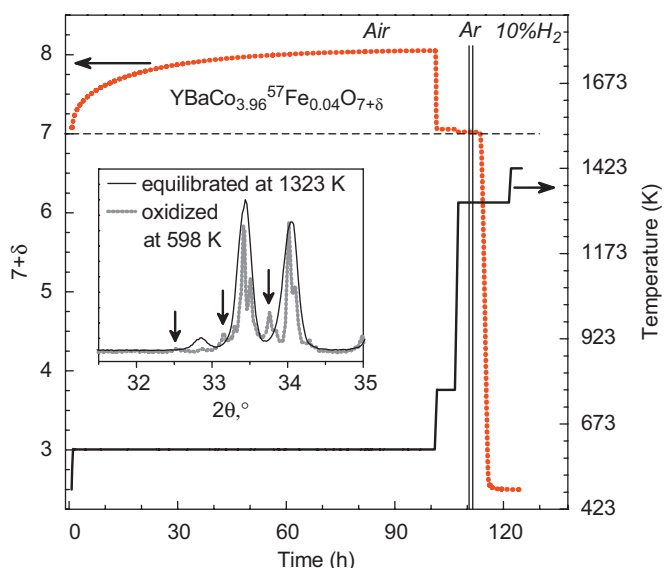

Fig. 2. Example of TGA curve illustrating the oxygen content variations during isothermal oxidation of $YBaCo_{3.96}$ $^{57}Fe_{0.04}O_{7+\delta}$ at 598 K in air, and the determination of total oxygen content by reduction into Y_2O_3, BaO, and metallic Co and Fe. Inset compares the characteristic fragments of XRD patterns of $YBaCo_{3.96}Fe_{0.04}O_{7.02}$ and $YBaCo_{3.96}Fe_{0.04}O_{7.80}$, showing the appearance of superstructure reflections (see text).

the second order Doppler shift. At 4 K, the sextet with larger B_{hf} may be assigned to the Co1 positions characterized by longer interatomic distances [8] and, hence, lower covalence of the Co–O bonds. The relationship between relative areas of the two contributions is moderately higher than the ideal Co1:Co2 concentration ratio (1:3), thus suggesting that Fe^{3+} distribution between the sites is not completely random, with a slight preference for the Co1 positions. Nonetheless, the extensive incorporation of Fe^{3+} cations into both cobalt sites unambiguously demonstrates an absence of charge ordering.

In the case of $YBaCo_{3.96}Fe_{0.04}O_{7.80}$ (Fig. 3b), introducing one additional doublet or sextet is necessary to adequately describe the spectra collected at high and low temperatures, respectively. The larger IS of this new component is indicative of Fe^{3+} states with a higher coordination, most likely octahedral, in accordance with structural data [3]. Within the limits of experimental uncertainty, the fraction of these iron–oxygen polyhedra is very close to $\frac{1}{4}$ (Table 1), which corresponds to the ratio of octahedral and tetrahedral cobalt sites in $YBaCo_4O_8$ [3]. At the same time, the total oxygen content in oxidized $YBaCo_{3.96}Fe_{0.04}O_{7.80}$ is lower than eight atoms per formula unit, displaying a higher affinity of Fe^{3+} cations for the formation of metal–oxygen octahedra with respect to cobalt due to the difference in average oxidation states. Moreover, the intercalation of extra oxygen in $YBaCo_{3.96}Fe_{0.04}O_{7+\delta}$ increases the fraction of Fe^{3+} located in the tetrahedrally coordinated Co1 sites if compared to Co2, although the relative concentrations of octahedra formed in both layers should be equal. These tendencies, and the extremely slow relaxation rate during oxidation (Fig. 2), all indicate a substantial structural reconstruction accompanied with Fe/Co cation re-distribution between the different crystallographic positions in $YBaCo_{3.96}Fe_{0.04}O_{7+\delta}$. In the narrow temperature range where $YBaCo_{3.96}Fe_{0.04}O_{7+\delta}$ can be oxidized without phase decomposition, the reconstruction rate should be governed by kinetically stagnated processes of short-range cation diffusion. For comparison, the isothermal TGA curves measured for iron-free $YBaCo_4O_{7+\delta}$ at 543–623 K tend to stabilize within a few hours [4,6]; annealing in flowing 20% O_2–N_2 gas mixture at 603 K leads to the formation of oxygen-hyperstoichiometric composition with $\delta = 1.1$ after 6 h. On the contrary, equilibration of $YBaCo_{3.96}Fe_{0.04}O_{7+\delta}$ is not fully achieved even after the isothermal treatment during more than 100 h at 598 K in air, although further heating leads to rapid oxygen desorption (Fig. 2). It should also be mentioned that the slow oxidation kinetics makes it possible to
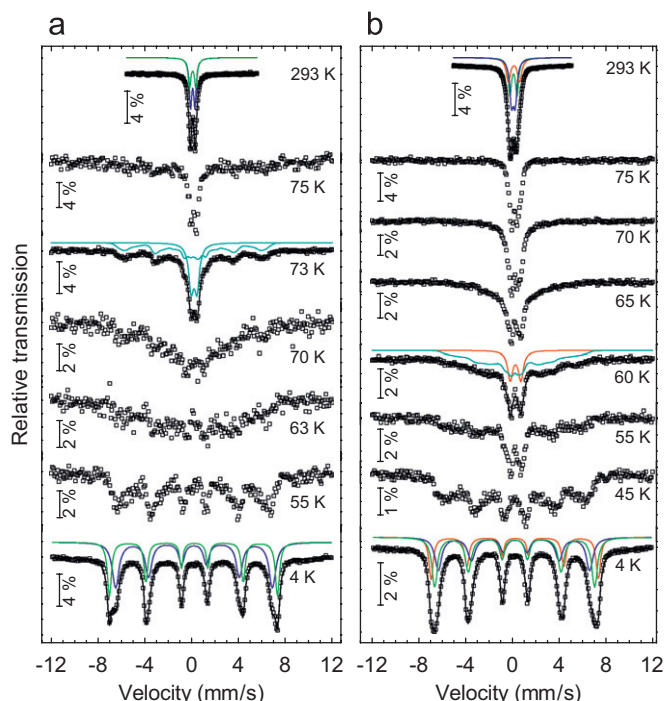
(Fig. 3a) were analyzed with two quadrupole doublets or two magnetic sextets, which correspond to the Co1 and Co2 crystallographic sites at 293 and 4 K, respectively. Any orthorhombic distortions leading to the separation of Co21, Co22 and Co23 positions in the case of $Pbn2_1$ space group [8] cannot be resolved by MS. The final estimated parameters at the highest and lowest temperatures are consistent with each other (Table 1). The isomer shifts (IS) of the two contributions are very similar, both typical for tetrahedrally coordinated high-spin Fe^{3+} in layered oxide phases [17]. Notice that no evidence for Fe^{2+} formation was observed. In combination with the minor hyperstoichiometry detected by TGA ($\delta = 0.02$), the latter fact reveals that the substitution of iron for cobalt is compensated exclusively by extra oxygen intercalation, without any effect on the Co^{2+}:Co^{3+} ratio. The decrease in IS values with increasing temperature is due to

Fig. 3. Selected Mössbauer spectra of $YBaCo_{3.96}$ $^{57}Fe_{0.04}O_{7.02}$ (a) and $YBaCo_{3.96}$ $^{57}Fe_{0.04}O_{7.80}$ (b). The lines plotted over experimental data points are the sum of two quadrupole doublets at 293 K, two magnetic sextets at 4 K, and the sum of one quadrupole doublet and a magnetic hyperfine field distribution at other temperatures. The subspectra are shown slightly shifted for clarity.

precisely control oxygen content in $YBa(Co,Fe)O_{7+\delta}$ by selecting appropriate duration of the thermal treatments.

When analyzing the oxygen intercalation effects on magnetic behavior, one should note that all tetrahedrally coordinated Fe^{3+} cations in $YBaCo_{3.96}Fe_{0.04}O_{7.02}$ exhibit a drastic reduction in relaxation frequency of the magnetic moments (μ_{Fe}) as temperature decreases from 75 K to 70 K (Fig. 3a). At 73 K one sextet and one doublet, both with broadened peaks, are observed. The quadrupole splitting (QS) of the latter signal is intermediate between the QS values at 293 K (Table 1), thus suggesting a synchronous behavior of both cobalt sublattices on cooling. Strong broadening of the sextet peaks is typical for relaxation of the μ_{Fe} directions with a frequency similar to the reciprocal observation time of the Mössbauer effect. Further cooling leads to frozen magnetic moments when the long-range magnetic correlations in both triangular and Kagomé layers are established. The magnetic freezing temperature of $YBaCo_{3.96}Fe_{0.04}O_{7.02}$ is lower than that for $YBaCo_4O_7$ [7], a result of disordering induced by the dopant cations and/or minor oxygen hyperstoichiometry.

A considerably different behavior is observed for oxidized $YBaCo_{3.96}Fe_{0.04}O_{7.80}$ (Fig. 3b), where only the tetra-coordinated iron cations show frozen magnetic moments below 70 K, while Fe^{3+} in octahedral coordination remain paramagnetic down to 55 K. This difference originates from the incorporation of additional oxygen ions forming zigzag chains of edge-sharing octahedra along the c axis of $YBaCo_4O_8$-type lattice [3], which disrupts the three-dimensional Co(Fe) tetrahedra network in one direction and distorts the Co(Fe)–O–Co(Fe) bond angles if

compared to the oxygen-stoichiometric phase, as illustrated by Fig. 1a–d. As a consequence, the exchange interactions become weaker and the long-range magnetic correlations are established at lower temperatures.

4. Conclusions

The substitution of 1% ^{57}Fe for cobalt in $YBaCo_4O_{7+\delta}$ was performed to probe local interactions and magnetic ordering phenomena in oxidized and essentially oxygen-stoichiometric lattices by the MS. Within the limits of experimental uncertainty, all iron cations were found trivalent, irrespective of the oxygen content varying in the range 7.02–7.80 atoms per formula unit as determined by TGA. Despite a modest tendency for preferential occupation of the triangular layers by Fe^{3+}, which becomes more pronounced in oxidized $YBaCo_{3.96}Fe_{0.04}O_{7.80}$, no evidence of charge ordering was revealed. Decreasing temperature below 75–80 K leads to gradual freezing of the iron magnetic moments. The formation of metal–oxygen octahedra and resultant structural distortions hinder magnetic interactions, extending the temperature range with co-existing paramagnetic and frozen states down to 45–50 K. Although the oxygen stoichiometry changes at 773 and 1323 K in air are characterized by relatively fast kinetics, the isothermal oxidation at 598 K is extremely slow, probably due to substantial structural reconstruction confirmed by the MS.

References

[1] D.V. Sheptyakov, A. Podlesnyak, S.N. Barilo, S.V. Shiryaev, D.D. Khalyavin, D.Yu. Chernyshov, N.I. Leonyuk, PSI Sci. Rep. 3 (2001) 64.
[2] M. Valldor, M. Andersson, Solid State Sci. 4 (2002) 923–931.
[3] O. Chmaissem, H. Zheng, A. Huq, P.W. Stephens, J.F. Mitchell, J. Solid State Chem. 181 (2008) 664–672.
[4] M. Karppinen, H. Yamauchi, S. Otani, T. Fujita, T. Motohashi, Y.-H. Huang, M. Valkeapää, H. Fjellvåg, Chem. Mater. 18 (2006) 490–494.
[5] A. Maignan, V. Caignaert, D. Pelloquin, S. Hébert, V. Pralong, Phys. Rev. B 74 (2006) 165110.
[6] H. Hao, J. Cui, C. Chen, L. Pan, J. Hu, X. Hu, Solid State Ionics 177 (2006) 631–637.
[7] L.C. Chapon, P.G. Radaelli, H. Zheng, J.F. Mitchell, Phys. Rev. B 74 (2006) 172401.
[8] A. Huq, J.F. Mitchell, H. Zheng, L.C. Chapon, P.G. Radaelli, K.S. Knight, P.W. Stephens, J. Solid State Chem. 179 (2006) 1136–1145.
[9] V. Caignaert, A. Maignan, V. Pralong, S. Hébert, D. Pelloquin, Solid State Sci. 8 (2006) 1160–1163.
[10] M. Soda, Y. Yasui, T. Moyoshi, M. Sato, N. Igawa, K. Kakurai, J. Magn. Magn. Mater. 310 (2007) e441–e442.
[11] M. Valkeapää, M. Karppinen, T. Motohashi, R.-S. Liu, J.-M. Chen, H. Yamauchi, Chem. Lett. 36 (2007) 1368–1369.
[12] E.V. Tsipis, V.V. Kharton, J.R. Frade, Solid State Ionics 177 (2006) 1823–1826.
[13] E.V. Tsipis, V.V. Kharton, J.R. Frade, P. Núñez, J. Solid State Electrochem. 9 (2005) 547–557.
[14] T. Motohashi, S. Kadota, H. Fjellvåg, M. Karppinen, H. Yamauchi, Mater. Sci. Eng. B 148 (2008) 196–198.
[15] S. Räsänen, H. Yamauchi, M. Karppinen, Chem. Lett. 37 (2008) 638–639.
[16] L.A. Chick, L.R. Pederson, G.D. Maupin, J.L. Bates, L.E. Thomas, G.J. Exarhos, Mater. Lett. 10 (1990) 6–12.
[17] J.C. Waerenborgh, D.P. Rojas, N.P. Vyshatko, A.L. Shaula, V.V. Kharton, I.P. Marozau, E.N. Naumovich, Mater. Lett. 57 (2003) 4388–4393.
[18] D. Predoi, V. Kuncser, E. Tronc, M. Nogues, U. Russo, G. Principi, G. Filoti, J. Phys. Condens. Matter 15 (2003) 1797–1811.